Desalination and Water Treatment
www.deswater.com

doi: 10.5004/dwt.2023.30092

315 (2023) 40–48
December

Evaluation of pressure-assisted forward osmosis for concentrating desalination brine: a feasibility study

Garudachari Bhadrachari*, Mansour Ahmed, Rajesha Kumar Alambi, Jibu Pallickel Thomas

Water Research Center, Kuwait Institute for Scientific Research, P.O. Box: 24885, Safat 13109, Kuwait, emails: garuda.achar@gmail.com; bgarudachari@kisr.edu.kw (G. Bhadrachari), mahmed@kisr.edu.kw (M. Ahmed), ralambi@kisr.edu.kw (R.K. Alambi), jithomas@kisr.edu.kw (J.P. Thomas)

Received 15 June 2023; Accepted 25 October 2023

ABSTRACT

The seawater desalination process yields a substantial amount of brine, which contains higher concentrations of dissolved solids compared to seawater. Various methods such as multi-stage flash distillation (MSF), multi-effect distillation (MED), and reverse osmosis (RO) are employed to produce freshwater. However, these technologies must effectively handle the large volume of brine generated in a sustainable manner. Two emerging techniques, namely zero liquid discharge (ZLD) and mineral extraction, offer potential solutions, but they are more economically viable for smaller quantities of brine with high mineral salt concentrations. Hence, there is an urgent requirement for desalination systems capable of producing highly concentrated brine. Recent literature suggests that forward osmosis (FO) technology utilizing Aquaporin biomimetic membranes has shown promising results for seawater desalination. To address this need, experimental investigations were performed to evaluate four commercially available FO membranes for brine concentration applications at different operating parameters such as flow rate and feed pressure. The study revealed that the Z-nano Aquaporin membrane achieved the highest water flux when groundwater RO brine is used as feed solution. Overall, the Aquaporin biomimetic membranes outperformed cellulose triacetate and (CTA) and thin film composite (TFC) membranes in brine concentration applications, demonstrating their superior performance.

Keywords: Aquaporin membrane; Desalination; Brine concentration; Forward osmosis; Water recovery

1. Introduction

Many countries particularly those in the Middle East, heavily depend on seawater for the desalination process [1–4]. Desalination plants utilize two main methods: thermal and membrane-based. The thermal process involves an evaporator and a condenser, which heat the feed seawater to a specific temperature, causing it to evaporate and then condense into freshwater. On the other hand, the membrane method utilizes high pressure and a membrane to separate salt and molecules from the seawater, producing freshwater without undergoing a phase shift [5,6]. Both of these desalination processes result in the production of a significant amount of brine as a by-product. The brine salinity generated by seawater reverse osmosis (SWRO) ranges from 60 to 85 g/L total dissolved solids (TDS) and has a lower temperature compared to the thermal process [7–9]. In thermal technologies like multi-stage flash (MSF) and multi-effect distillation (MED), the brine produced has a TDS range of 55–65 g/L [8]. Various methods are employed to manage and dispose of desalination brine, including deep well injection, surface water disposal, irrigation of

* Corresponding author.

salt-tolerant plants, dumping into municipal sewers, and evaporation ponds. However, it is important to mention that all of these technologies pose environmental hazards and come at a high cost [10–13].

Several technologies for concentrating desalination brine have been developed and demonstrated at pilot and demonstration scales [14–17]. However, these technologies require significant energy consumption and substantial capital investment, preventing their commercialization [18,19]. Among the smaller-scale processes, membrane distillation (MD), forward osmosis (FO), and pressure-assisted forward osmosis (PAFO) have shown promising results for brine concentration. FO offers the advantage of low energy requirements, while MD has the capability to utilize low-quality energy or waste heat, in addition to being compatible with renewable energy sources. [9,12,17,20–22]. PAFO has emerged as a favourable option due to its higher water flux and salt rejection compared to FO and MD processes [17,22]. Previous studies have demonstrated that applying mild pressure on the feed side of FO enhances both water flux and water recovery [23–26]. Based on the promising results from our previous research on biomimetic membranes in FO, further investigations were conducted into brine concentration applications using FO membranes in a pressure-assisted FO process [27–30].

2. Experimental section

2.1. Material and methods

The biomimetic membranes were acquired from Z-Nano Water Tech in California and Aquaporin A/S in Denmark. Hydration Technologies Innovation, USA, supplied cellulose triacetate (CTA) and thin-film composite cellulose triacetate (TFC CTA) membranes. Draw solution (DS) was prepared by dissolving 26% sodium chloride (NaCl) in deionized (DI) water. Samples of the feed solution (RO brine) were collected from various sources, including the Desalination Research Plant (DRP) at Kuwait Institute for Scientific Research Doha campus, Shuwaikh RO (SRO), Shuwaikh MSF (SMSF) facilities, and ground water RO brine (GWRO) from Abdali Farm Kuwait. The brine samples were obtained from 25 L plastic tanks and subjected to testing using state-of-the-art water analysis instruments. Calcium and magnesium were measured using the ethylenediaminetetraacetic acid (EDTA) titration method, while sulphate was measured using spectrophotometer LANGE DR2800. The THERMO SCIENTIFIC, iCAP 6000 was used to assess the other elements found in all brine samples. Table 1 shows the mineral salt concentrations in collected brine samples. At the Desalination Research Plant (DRP), the seawater feed supply to the RO plant is obtained from a beach-well. On the other hand, the RO plant at Shuwaikh receives its feed water directly from the sea. Due to variations in the quality of input water and the percentage of freshwater recovery, the RO process at both the DRP and Shuwaikh desalination plants generates brine with different salt concentrations. Fig. 1 shows a schematic illustration of the PAFO system. Fig. 2 depicts the laboratory scale PAFO system obtained from Trevi Systems, California. The system is capable of operate at varying flow rates and applied pressures of up to 2 bar.

2.2. Characterization of membranes

All the membranes selected for the experiments were characterized using the following instruments: a Goniometer for measuring water contact angle (WCA), an EVO MA18 instrument with Oxford EDS(X-act) for examining surface morphology through field emission scanning electron microscopy (FESEM), and a nano-observer instrument for analyzing topology through atomic force microscopy (AFM). The topography was evaluated by scanning a section of the membrane with dimensions of 10 × 10 μm.

2.3. Experimental procedure for pressure assisted forward osmosis experiments

PAFO tests were carried out using laboratory-scale cross flow filtration equipment, as shown in Fig. 2. The plate-and-frame cross-flow permeation cell has a rectangular channel on each side of the membrane. During the PAFO testing, different flow rates of both the feed solution (FS) and draw solution (DS) were examined while keeping their respective flow rates constant. The FS and DS were pumped through the membrane using the concurrent flow technique. The temperatures and DS concentrations remained constant throughout the experiment at 25°C and 26%, respectively. The active layer of the membrane was kept facing FS, and

Table 1
Chemical composition of reverse osmosis and multistage flash distillation brine

Parameters/Unit	DRP RO brine	SRO brine	SMSF brine	gwro brine
TDS (ppm)	54,900	64,110	79,514	14,240
pH	7.13	7.14	8.3	8.13
Conductivity (mS/cm)	69.4	76.79	84.4	21.5
Magnesium (mg/L)	1,673	2,763	2,787	436
Calcium (mg/L)	1,090	1,120	920	1,372
Sulfate (mg/L)	4,159	6,832	6,608	2,630
Sodium (mg/L)	17,905	28,316	23,208	4,226
Chloride (mg/L)	35,212	47,732	42,862	6,514

TDS: Total dissolved solid, DRP RO: Desalination research plant reverse osmosis, SRO: Shuwaikh reverse osmosis, SMSF: Shuwaikh multistage flash, GWRO: Ground water reverse osmosis.

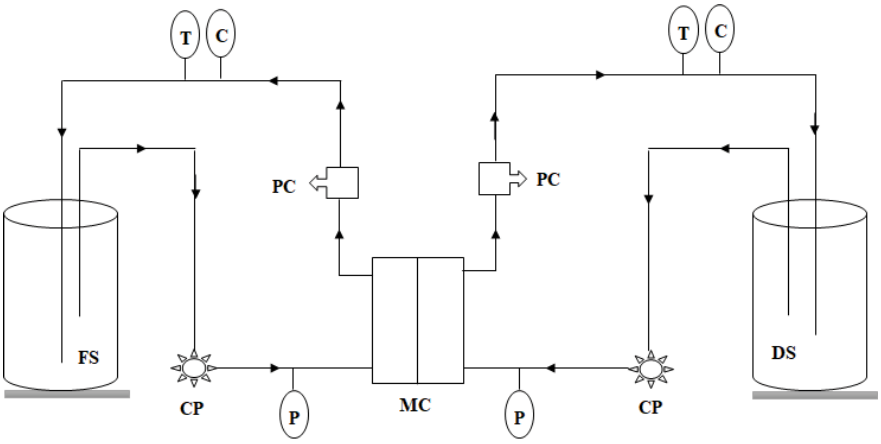

Fig. 1. Schematic diagram of pressure assisted forward osmosis system.

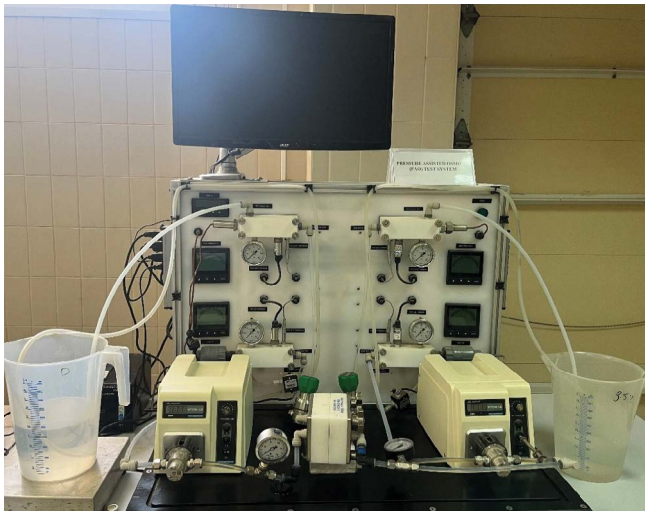

Fig. 2. Laboratory scale pressure-assisted forward osmosis system.

pressure was applied to the FS side by pressure regulator. The concentration and flow of feed and draw solution, as well as the flow of water across the membrane, were measured both automatically and manually. The system was operated for duration of 130 min, with data points being recorded after 10 min of initiating the experiment. The desalination performance parameter of PAFO trials was determined using Eqs. (1)–(3) [31]:

$$J_w = \left(\frac{V_{\mathrm{Fi}} - V_{\mathrm{Ff}}}{A_m \times t} \right) \tag{1}$$

where J_w: water flux; V_{Ff}: feed final volume; V_{Fi}: feed initial volume; A_m: membrane area; t: duration of process.

$$R_y = \left(1 - \frac{V_{\mathrm{Ff}}}{V_{\mathrm{Fi}}} \right) \tag{2}$$

where R_y: feed recovery; V_{Ff}: feed final volume; V_{Fi}: feed initial volume.

$$R_c = \left(\frac{C_{\mathrm{Df}} V_{\mathrm{Df}} - C_{\mathrm{Di}} V_{\mathrm{Di}}}{\left(C_{\mathrm{Ff}} - C_{\mathrm{Fi}} / 2 \right) \times \left(V_{\mathrm{Df}} - V_{\mathrm{Di}} \right)} \right) \tag{3}$$

where R_c: salt rejection, C_{Df}: final draw solution concentration; V_{Df}: final draw solution volume; C_{Di}: initial draw solution concentration; V_{Di}: initial draw solution volume; C_{Ff}: final feed solution concentration; C_{Fi}: initial feed solution concentration.

3. Results and discussion

3.1. Characterization

3.1.1. Water contact angle and topological studies of membranes

The WCA of commercial CTA, TFC, AqZ, and Z-nano membranes was measured using the sessile droplet method [32]. In this study, a water droplet was carefully placed on the membrane surface using a micro syringe to measure the WCA until no further change was observed. The measurement was conducted at five different locations on a 1 cm^2 area of the membrane sample, and the average value was reported. Topological investigations of membranes were conducted using AFM, which entailed measuring the varied surface characteristics of the membrane.

The WCA results showed lowest value for AqZ membrane compared with CTA, TFC, and Z-nano membranes. The order of WCA obtained was Z-nano (59.33°) > TFC (37°) > CTA (36.5°) > AqZ (24.83°). The variations in the WCA of the membrane could be attributed to the nature of the polymer's chemical composition and the way it is fabricated. The AFM study shows that the CTA membrane has the highest average roughness compared to the TFC, Aquaporin, and Z-nano membranes. The order of maximum roughness is as follows: CTA > Aqz > Z-nano > TFC. The maximum average roughness measured for the CTA membrane is 3,955 nm, while the lowest is 912 nm for the TFC membrane. Fig. 3 displays surface AFM images of the commercial CTA, TFC, AqZ, and Z-nano membranes, while Table 2 presents the WCA and surface roughness parameters such as maximum mean roughness (R_a), route mean square roughness (R_q), and maximum feature height (R_{max}).

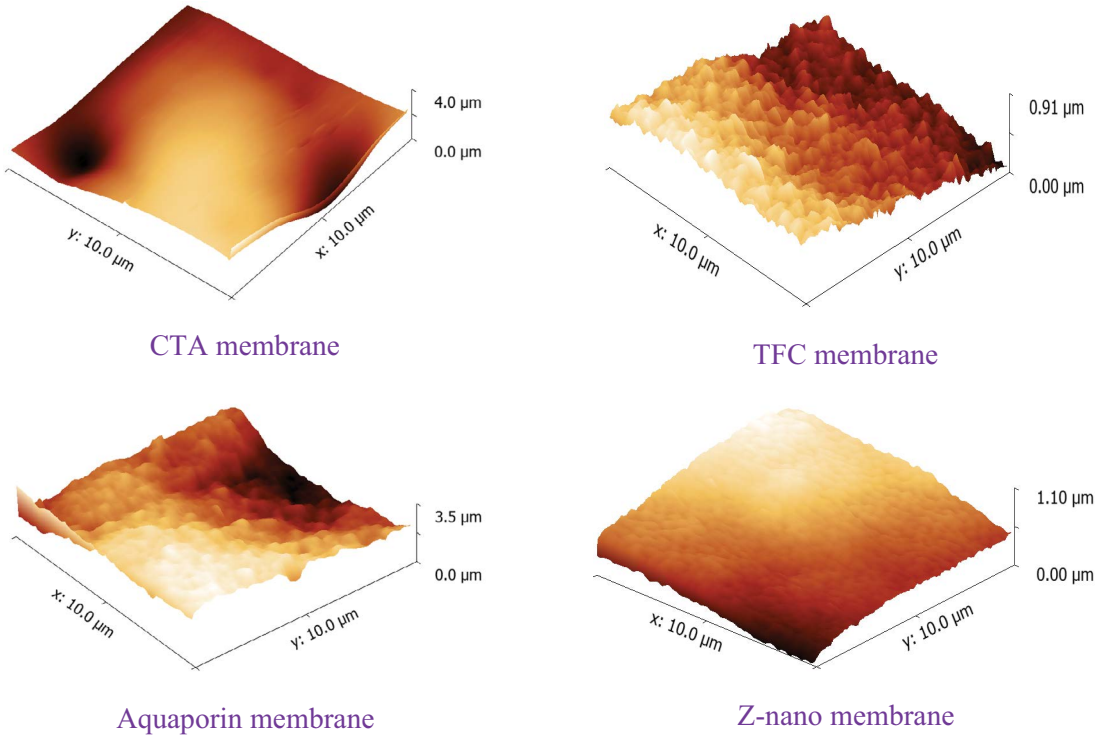

Fig. 3. Three-dimensional AFM images of cellulose triacetate, thin-film composite, aquaporin, and Z-nano membranes.

Table 2
Water contact angle, surface roughness parameters of cellulose triacetate, thin-film composite, aquaporin, and Z-nano membranes

Membrane code	WCA (°)	R_a (nm)	R_{ms} (nm)	Maximum (nm)	Average (nm)
CTA	36.5	340	307	3,955	716
TFC	37	157	183	912	429.8
AqZ	24.83	60.5	89.5	2,601.7	315.3
Z-nano	59.33	186	221	1,103	618

Cellulose triacetate (CTA), thin-film composite (TFC), aquaporin (AQZ), and Z-nano, water contact angle (WCA), maximum mean roughness (R_a), route mean square roughness (R_q) and maximum feature heights (R_{max}).

3.1.2. Morphological studies of membranes

Prior to conducting FESEM (field emission scanning electron microscope) analysis, all the membranes were subjected to drying. Subsequently, the dried membrane samples were cryogenically fractured using liquid nitrogen and fixed to a metallic base using double-sided carbon tape. To enhance conductivity and obtain clearer FESEM images, a thin layer of gold was applied to the membrane surface using the agar manual sputter coater (AGB7340). Once these preparatory steps were completed, the morphology of the membranes was examined. The TFC membrane had a consistent but smaller pore size compared to the CTA, AqZ, and Z-nano membranes. The CTA membrane exhibited a fibrous structure with uneven pore sizes, whereas the AqZ membrane featured pores ranging from 310 to 490 nm in size. The FESEM image of the Z-nano membrane was very clear and had a pore size of less than 100 nm, showing a uniform distribution. The uniform pore distribution of the TFC and Z-nano membranes could be attributed to a uniform selective layer coating on the substrate membrane [33]. Fig. 4 displays the FESEM images of the commercial CTA, TFC, AqZ, and Z-nano membranes.

3.2. Desalination performance study

The PAFO desalination performance trials were carried out utilizing four distinct flat sheet membranes. The influence of operating parameters on brine concentration application was investigated by adjusting operating parameters such as applied pressure, flow rate, and feed concentrations.

3.2.1. Effect of feed pressure on water flux, water recovery and salt rejection

The experiments conducted by PAFO involved varying the feed side pressure from 0 to 1.5 bar, while maintaining a constant flow rate of 750 mL/min for both the feed solution (FS) and draw solution (DS), and a temperature of 25°C.

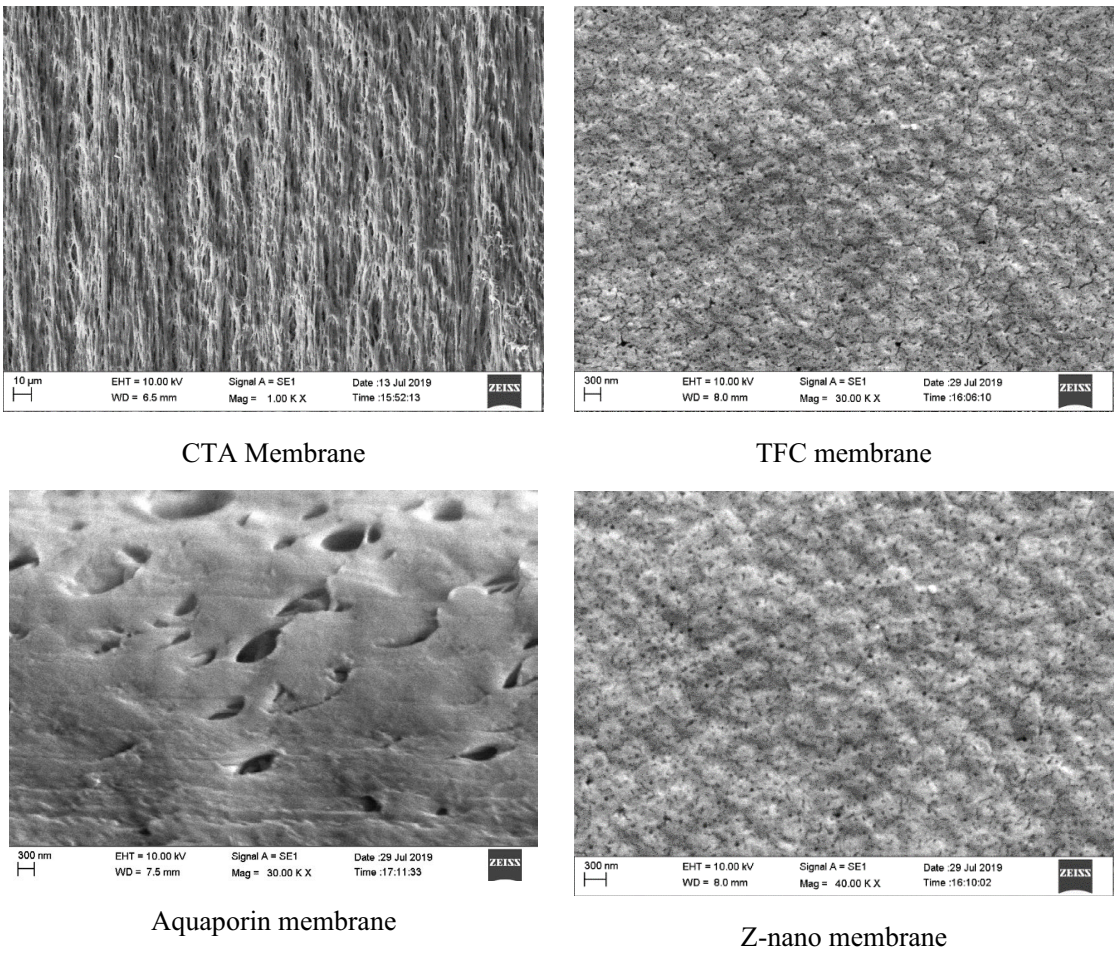

Fig. 4. Magnified surface field emission scanning electron microscopy images of commercial cellulose triacetate, thin-film composite, aquaporin, and Z-nano membranes.

The feed used in the experiments was the RO brine from the DRP RO plant without any treatments or additives. The results of the experiments showed that the water flux increased with an increase in the applied pressure on the feed side. This could be attributed to the additional hydraulic pressure in combination with the osmotic pressure of the draw solution. The TFC membrane showed the lowest water flux compared to the CTA, Aquaporin, and Z-nano membranes. This difference in performance can be attributed to factors such as smaller pore size, less hydrophilicity, pore distribution, and membrane morphology of the CTA membrane. On the other hand, the Aquaporin membrane showed moderate water flux, and the Z-nano membrane demonstrated excellent water flux. Both the Aquaporin and Z-nano membranes are biomimetic in nature, and have a biological water transport active structure in its TFC layer. These biomimetic membranes have specialized pore structures that facilitate selective water molecule transport, leading to their improved water flux compared to CTA and TFC membranes. Fig. 5 illustrates the variation in water flux with respect to the applied feed pressure for different membranes.

The water recovery showed a similar trend to the water flux, as shown in Fig. 6. The findings for all the examined membranes revealed that higher feed pressure led to increased water recovery. On the other hand, the salt rejection exhibited an inverse pattern, with increasing feed pressure resulting in decreased salt rejection. This suggests that the rise in pressure on the feed side contributes to salt leakage. One possible explanation is that the CTA and TFC membranes have larger pore sizes compared to ionized salts. In the case of biomimetic membranes, this phenomenon could be attributed to aquaporin pore degradation or enhancement. Fig. 7 shows the salt rejection capabilities of the tested membranes. Overall, the results reveal that 0.5 bar is better for obtaining moderate water flux, recovery, and high salt rejection.

3.2.2. Effect of feed and draw solution flow rate on water flux, water recovery, and salt rejection

The impact of flow rate on performance indicators such as water flux, water recovery, and salt rejection were investigated while maintaining a constant temperature of 25°C, draw solution (DS) concentration of 26%, and feed pressure of 0.5 bar. The flow rate was adjusted equally on both sides of the membrane, reaching 500, 750, and 1,000 mL/min by increasing the frequencies of the feed solution

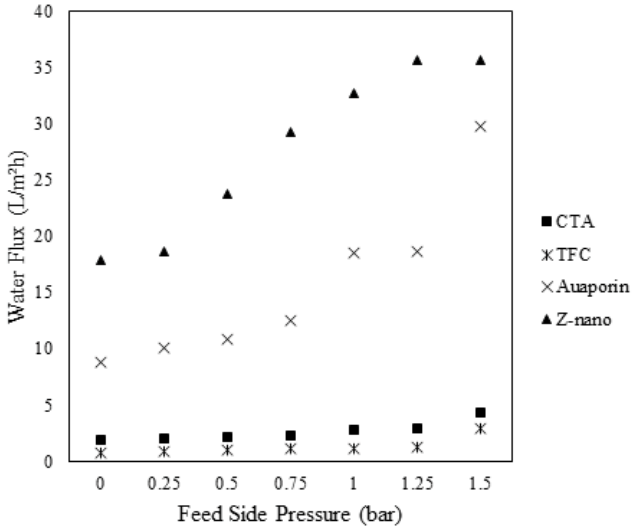

Fig. 5. Impact of applied feed pressure on water flux.

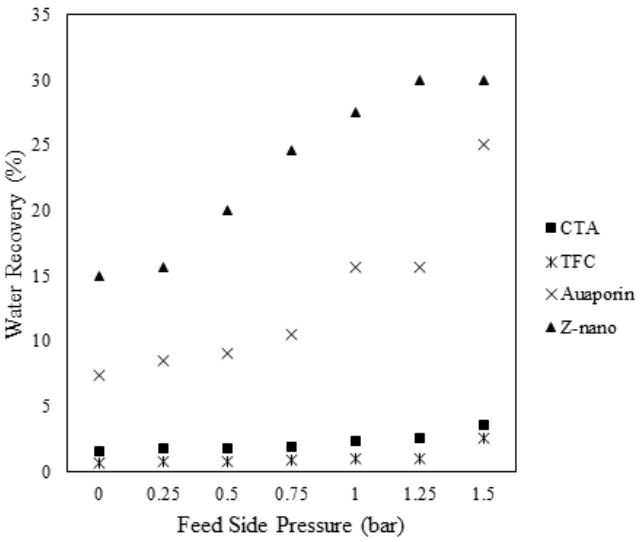

Fig. 6. Impact of applied feed pressure on water recovery.

(FS) and DS pumps. The results demonstrated a gradual increase in water flux and recovery as the flow rate was increased from 500 to 1,000 mL/min. Figs. 8 and 9 illustrate the water flux and water recovery at different flow rates, respectively. Fig. 10 illustrates the promising salt rejection percentages achieved by all the tested membranes, except for the CTA membrane. The enhanced water flux associated with higher flow rates can be attributed to a narrower concentration barrier across the membrane, leading to a greater osmotic pressure difference between the FS and DS. Consequently, water flux and recovery are increased. The lower salt rejection observed for the CTA membrane may be attributed to its larger pore size and increased shear forces on the membrane surface. However, at a flow rate of 750 mL/min, all the tested membranes exhibited superior performance in terms of water flux, water recovery, and salt rejection.

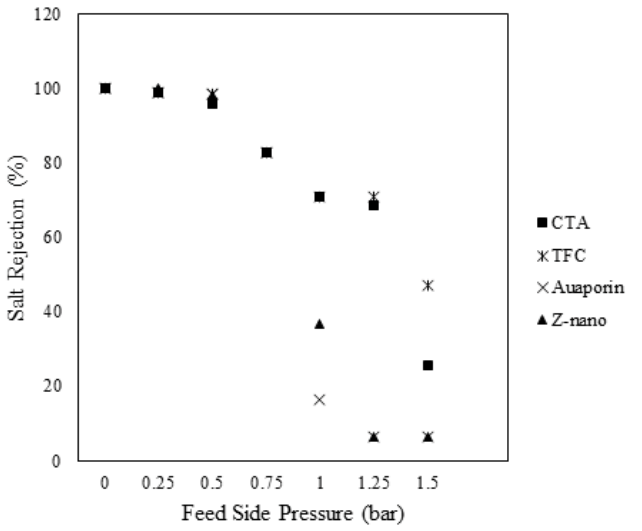

Fig. 7. Impact of applied feed pressure on salt rejection.

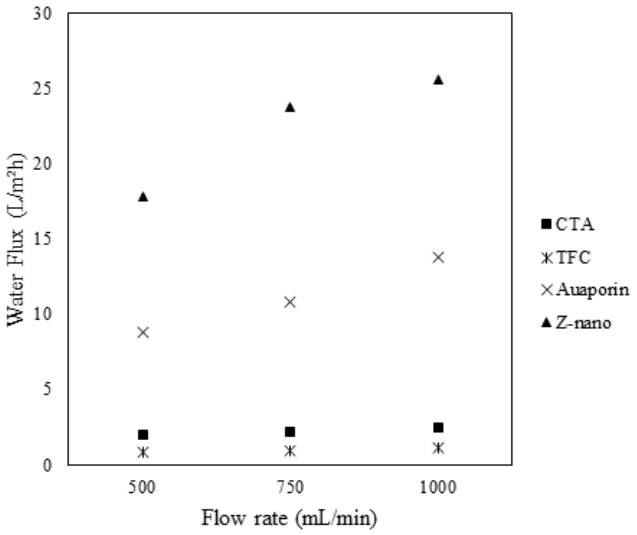

Fig. 8. Impact of flow rate on water flux.

3.2.3. Influence of varied feed compositions on water flux, water recovery, and salt rejection

The experiments were conducted using brine collected from various desalination plants in Kuwait, and its composition can be found in Table 1. In accordance with the optimal flow rates and feed pressure obtained from the previous sections, the experiments were conducted under carefully controlled conditions, ensuring a consistent temperature, flow rate, and feed side pressure throughout the study. The results shown in Figs. 11–13 clearly demonstrate how the salt content in the feed solution affects water flux, recovery, and salt rejection, respectively. Higher salt concentrations in the feed solution resulted in lower water flux and recovery rates. Notably, regardless of the specific feed solution used, a consistently high salt rejection rate of over 92% was achieved. Among the different feed solutions tested, the GWRO brine feed yielded the highest water

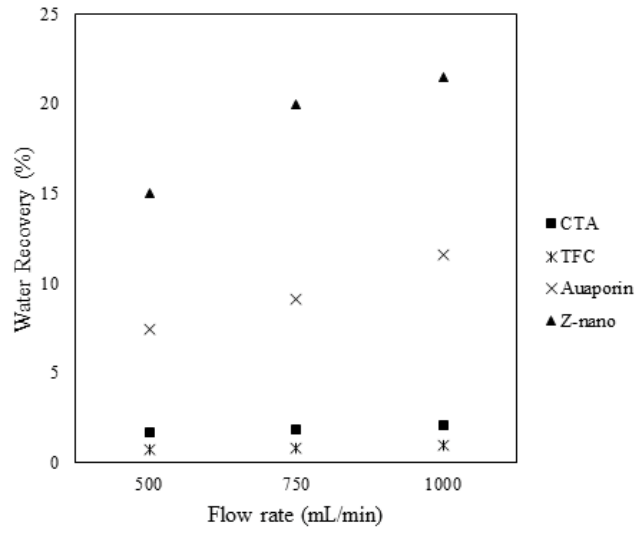

Fig. 9. Impact of flow rate on water recovery.

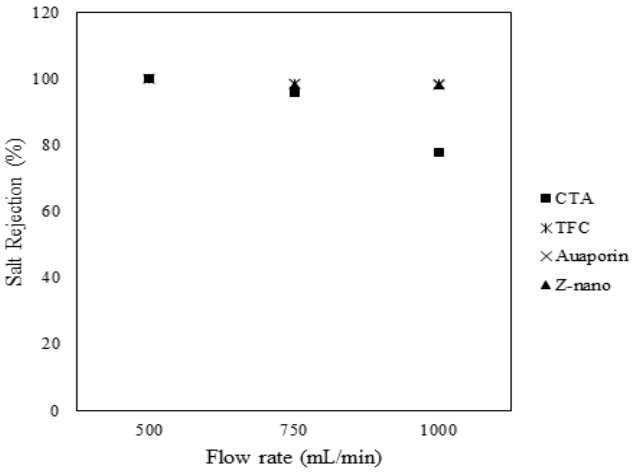

Fig. 10. Impact of flow rate on salt rejection.

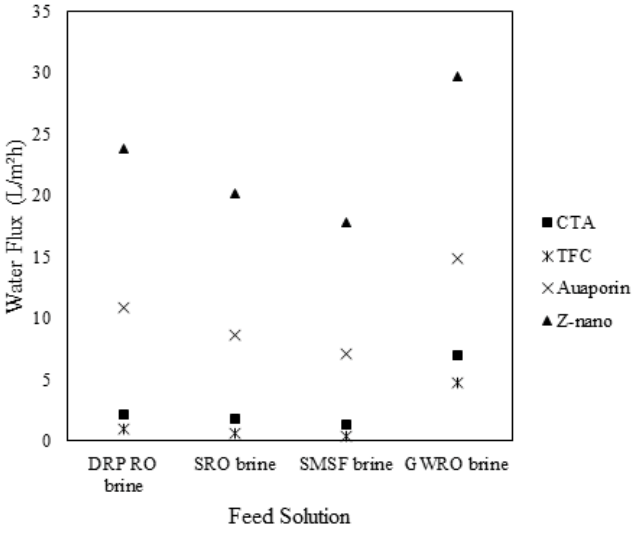

Fig. 11. Impact of feed concentration on water flux.

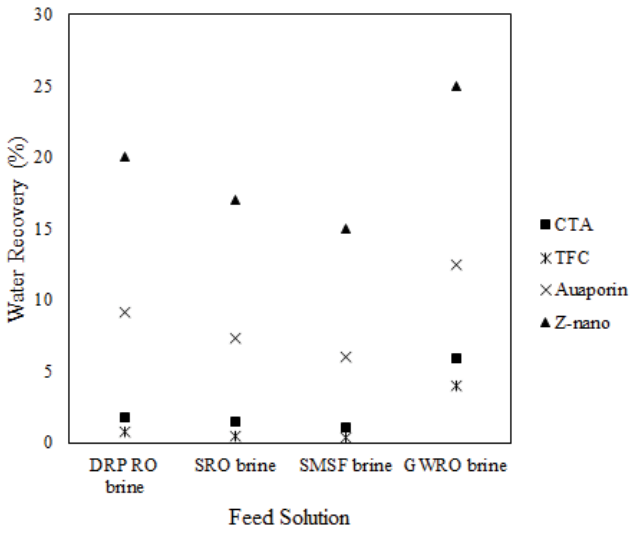

Fig. 12. Impact of feed concentration on water recovery.

flux of 29.7 L/m²·h when using the Z-nano membrane. The water flux rankings for the groundwater RO brine feed were as follows: TFC < CTA < Aquaporin < Z-nano. Conversely, the Shuwaikh MSF brine feed resulted in the lowest water flux, measuring 17.8 L/m²·h when employing the Z-nano membrane. The lower water flux observed with the MSF brine feed can be attributed to its higher total dissolved solids (TDS) content, as indicated in Table 1. In terms of desalination performance, the PAFO trial outcomes demonstrated that the Z-nano and Aquaporin membranes exhibited superior performance compared to the CTA and TFC membranes. This improved water permeability in biomimetic membranes may be attributed to their hydrophilicity, membrane thickness, and biological water transport channels.

4. Conclusions

The experimental study was conducted using brines collected from different desalination plants located at Kuwait to evaluate the feasibility of the pressure-assisted forward osmosis (PAFO) technique for brine concentration, employing four different types of FO membranes. The investigation involved varying operating conditions, such as applied pressure and feed flow rate, in order to identify the optimal conditions based on water flux, water recovery, and salt rejection. The results revealed that increasing the feed pressure resulted in higher water flux and water recovery rates, but diminished salt rejection. There was not much difference in the water flux between the CTA and TFC membranes when the feed pressure was increased from 0.75 to 1.50 bar. However, the Aquaporin membrane showed an increase in water flux from 12.5 to 29.7 L/m²·h when the feed pressure was increased from 0.75 to 1.50 bar. Similarly, the Z-nano membrane had an increase in water flow from 29.28 to 35.71 L/m²·h when the feed pressure was increased from 0.75 to 1.50 bar. In all the tested membranes, the rejection of salt decreased

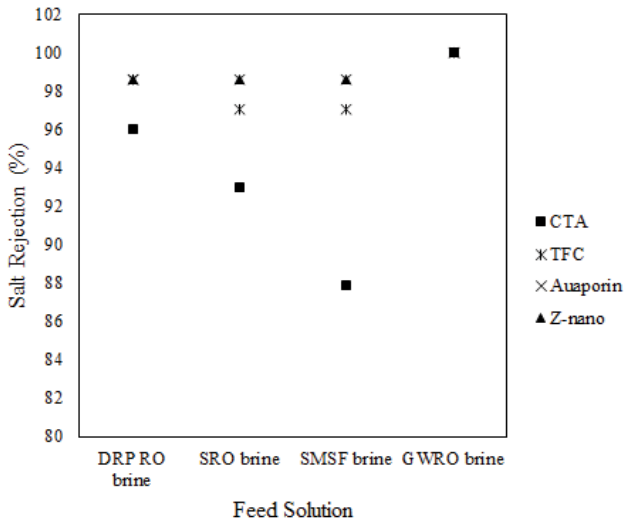

Fig. 13. Impact of feed concentration on salt rejection.

significantly when the pressure was increased from 0.75 to 1.50 bar. Similarly, when the feed flow rate was increased, a similar effect was seen in all the tested membranes. The highest water flux rate observed was 29.7 L/m^2·h (with a water recovery rate of 25%) and a salt rejection of 100% for the Z-nano membrane when using ground water RO brine as the feed solution. Among the membranes studied, the Z-nano membrane exhibited the highest water flux, water recovery, and salt rejection, surpassing the CTA, TFC, and Aquaporin membranes. Furthermore, biomimetic membranes such as the Z-nano and Aquaporin demonstrated superior performance in brine concentration compared to conventional CTA and TFC membranes. In conclusion, the findings from this study suggest that the pressure-assisted forward osmosis technique holds promise as a viable approach for desalination and brine concentration.

Acknowledgments

The authors express their gratitude to the Kuwait Institute for Scientific Research (KISR) for providing funding and valuable assistance throughout the completion of this research. The authors are sincerely thankful for their valuable contribution.

References

[1] B. Moossa, P. Trivedi, H. Saleem, S.J. Zaidi, Desalination in the GCC countries - a review, J. Cleaner Prod., 357 (2022) 131717, doi: 10.1016/j.jclepro.2022.131717.
[2] E. Jones, M. Qadir, M.T. van Vliet, V. Smakhtin, S.M. Kang, The state of desalination and brine production: a global outlook, Sci. Total Environ., 657 (2019) 1343–1356.
[3] J. Eke, A. Yusuf, A. Giwa, A. Sodiq, The global status of desalination: an assessment of current desalination technologies, plants and capacity, Desalination, 495 (2020) 114633, doi: 10.1016/j.desal.2020.114633.
[4] Z. Ai, F. Ishihama, N. Hanasaki, Mapping current and future seawater desalination plants globally using species distribution models, Water Resour. Res., 58 (2022) 1–13, doi: 10.1029/2021wr031156.
[5] A.F. Ismail, M.A. Rahman, M.H. Dzarfan Othman, T. Matsuura, Eds., Membrane Separation Principles and Applications: From Material Selection to Mechanisms and Industrial Uses, Edition Number 1, Elsevier, 2018, pp. 1–481, doi: 10.1016/C2016-0-04031-7.
[6] Y. Cohen, Advances in Water Desalination Technologies, Y. Cohen, Ed., Materials and Energy, Vol. 17, 2021, pp. 1–652.
[7] H.D. Ibrahim, E.A.B. Eltahir, Impact of brine discharge from seawater desalination plants on Persian/Arabian Gulf Salinity, J. Environ. Eng., 145 (2019) 1–12.
[8] A. Panagopoulos, K.J. Haralambous, Environmental impacts of desalination and brine treatment - challenges and mitigation measures, Mar. Pollut. Bull., 161 (2020) 1–12.
[9] S.N. Backer, I. Bouaziz, N. Kallayi, R.T. Thomas, G. Preethikumar, M.S. Takriff, T. Laoui, M.A. Atieh, Review: brine solution: current status, future management and technology development, Sustainability, 4 (2022) 1–47.
[10] D. Ghernaout, Desalination engineering: environmental impacts of the brine disposal and their control, OALib., 8 (2020) 1–17.
[11] A. Panagopoulos, K.J. Haralambous, M. Loizidou, Desalination brine disposal methods and treatment technologies - a review, Sci. Total Environ., 693 (2019) 1–23.
[12] D. Xevgenos, M. Marcou, V. Louca, E. Avramidi, G. Ioannou, M. Argyrou, P. Stavrou, M. Mortou, F. Küpper, Aspects of environmental impacts of seawater desalination: Cyprus as a case study, Desal. Water Treat., 211 (2021) 15–30.
[13] M. Omerspahic, H. Al-Jabri, S.A. Siddiqui, I. Saadaoui, Characteristics of desalination brine and its impacts on marine chemistry and health, with emphasis on the Persian/Arabian gulf: a review, Front. Mar. Sci., 9 (2022) 1–12.
[14] A. Giwa, V. Dufour, F. Al Marzooqi, M. Al Kaabi, S. Hasan, Brine management methods: recent innovations and current status, Desalination, 407 (2017) 1–23.
[15] T.V. Bartholomew, L. Mey, J.T. Arena, N.S. Siefert, M.S. Mauter, Osmotically assisted reverse osmosis for high salinity brine treatment, Desalination, 421 (2017) 3–11.
[16] Y. Choi, G. Naidu, L.D. Nghiem, S. Lee, S. Vigneswaran, Membrane distillation crystallization for brine mining and zero liquid discharge: opportunities, challenges, and recent progress, Environ. Sci. Water Res. Technol., 5 (2019) 1202–1221.
[17] A.S. Al-Amoudi, S. Ihm, A.M. Farooque, E.S. Al-Waznani, N. Voutchkov, Dual brine concentration for the beneficial use of two concentrate streams from desalination plant - concept proposal and pilot plant demonstration, Desalination, 564 (2023) 1–15.
[18] O. Ogunbiyi, J. Saththasivam, D. Al-Masri, Y. Manawi, J. Lawler, X. Zhang, Z. Liu, Sustainable brine management from the perspectives of water, energy and mineral recovery: a comprehensive review, Desalination, 513 (2021) 115055, doi: 10.1016/j.desal.2021.115055.
[19] M. Yaqub, W. Lee, Zero-liquid discharge (ZLD) technology for resource recovery from wastewater: a review, Sci. Total Environ., 681 (2019) 551–563.
[20] H.R. Lotfy, J. Stas, H. Roubík, Renewable energy powered membrane desalination - review of recent development, Environ. Sci. Pollut. Res., 29 (2022) 46552–46568.
[21] S. Kalogirou, Seawater desalination using renewable energy sources, Prog. Energy Combust. Sci., 31 (2005) 242–281.
[22] B.A. Sharkh, A.A. Al-Amoudi, M. Farooque, C.M. Fellows, S. Ihm, S. Lee, S. Li, N. Voutchkov, Seawater desalination concentrate - a new frontier for sustainable mining of valuable minerals, npj Clean Water, 5 (2022), doi: 10.1038/s41545-022-00153-6.
[23] D. Khanafer, S. Yadav, N. Ganbat, A. Altaee, J. Zhou, A.H. Hawari, Performance of the pressure assisted forward osmosis-MSF hybrid desalination plant, Water, 13 (2021) 1–16.
[24] H.M.B. Beigi, S. Gadkari, J. Sadhukhan, Osmotically assisted reverse osmosis, simulated to achieve high solute concentrations, at low energy consumption, Sci. Rep., 12 (2022) 1–12.
[25] N.A. Yaranal, S. Kumari, S. Narayanasamy, S. Subbiah, An analysis of the effects of pressure-assisted osmotic backwashing on the high recovery reverse osmosis system, J. Water Supply Res. Technol. AQUA, 69 (2019) 298–318.

[26] T. Yun, Y.J. Kim, S. Lee, S. Hong, G.I. Kim, Flux behavior and membrane fouling in pressure-assisted forward osmosis, Desal. Water Treat., 52 (2013) 564–569.
[27] A. Al-Sairafi, G. Bhadrachari, M. Ahmed, S.B. Al-Muqahwi, M. Al-Rughaib, Comparative study of commercially available biomimetic membrane performance for seawater desalination, Desal. Water Treat., 76 (2022) 62–69.
[28] R. Kumar, A.M. Isloor, A. Ismail, T. Matsuura, Synthesis and characterization of novel water soluble derivative of chitosan as an additive for polysulfone ultrafiltration membrane, J. Membr. Sci., 440 (2013) 140–147.
[29] R. Kumar, M. Ahmed, B. Garudachari, J.P. Thomas, Synthesis and evaluation of nanocomposite forward osmosis membranes for Kuwait seawater desalination, Desal. Water Treat., 176 (2020) 273–279.
[30] M. Ahmed, Y. Al-Wazzan, R. Kumar, B. Garudachari, J.P. Thomas, A comparative study of two different forward osmosis membranes tested using pilot-plant system for Arabian Gulf seawater desalination, Desal. Water Treat., 176 (2020) 252–259.
[31] D.D.W. Rufuss, E. Hosseinipour, S. Arulvel, P. Davies, Complete parametric investigation of a forward osmosis process using sodium chloride draw solution, Desalination, 547 (2023) 116218, doi: 10.1016/j.desal.2022.116218.
[32] M. Ponomar, E. Krasnyuk, D. Butylskii, V. Nikonenko, Y. Wang, C. Jiang, T. Xu, N. Pismenskaya, Sessile drop method: critical analysis and optimization for measuring the contact angle of an ion-exchange membrane surface, Membranes, 12 (2022) 1–21.
[33] L. Xia, M.F. Andersen, C. Hélix-Nielsen, J.R. McCutcheon, Novel commercial aquaporin flat-sheet membrane for forward osmosis, Ind. Eng. Chem. Res., 56 (2017) 11919–11925.